Materials Research. 2026; 29: e20250572
DOI: https://doi.org/10.1590/1980-5373-MR-2025-0572

Sustainable and Innovative Permeable Ceramic Pavements from Mineral Processing Waste

Ricardo E. B. Ramos Filho[a]*, Augusto S. Oliveira[a], Déborah dos S. Gomes[a], Hellen C. T. Firmino[a], Josenildo I. dos Santos Filho[a], Romualdo R. Menezes[a], Gelmires de A. Neves[a]

[a]Universidade Federal de Campina Grande, Centro de Ciências e Tecnologia, Unidade Acadêmica de Engenharia de Materiais, Av. Aprígio Veloso, 882, Bodocongó, 58429-900, Campina Grande, PB, Brasil.

Received: July 30, 2025; Revised: November 12, 2025; Accepted: December 17, 2025

One of the solutions to flooding problems, especially in large cities, is the use of permeable pavements that can be produced using mineral waste, reducing costs and environmental impacts, and generating a circular economy. In this study, wastes from the exploitation and processing of kaolin, scheelite, and granite were used to produce ceramic permeable pavements. After characterization, the mineral wastes were mixed with a commercial red clay with samples uniaxially pressed (20 MPa) and sintered at 1050, 1100 and 1150 °C, with a heating rate of 5 °C/min. The formulations of kaolin processing residues sintered at 1050 °C and scheelite processing residues sintered at 1100 °C stand out with the highest porosity (close to 40%), high permeability (up to 7.42×10^{-4} m/s) and flexural strength ranging from 2.45 to 4MPa. These results emphasize the role of formulation parameters, highlighting the potential of ceramic permeable pavements as a high-performance, cost-effective, and sustainable solution.

Keywords: *permeable pavement, ceramic pavement, mineral wastes, storm drainage, sustainable innovation.*

1. Introduction

Stormwater management in several cities around the world is based on centralized systems, evacuating runoff as quickly as possible through drainage networks that collect and conduct runoff to the final treatment point or receiving water body. Among these sustainable techniques, permeable pavements represent an effective solution to reduce stormwater runoff and provide pollutant treatment. These pavements are passable surfaces for both pedestrians and vehicles that allow water to filter, enabling infiltration, groundwater recharge or water reuse[1] and can intercept more than 50% of the total rainfall volume during rain events[2]. In addition, permeable materials generally have characteristics such as porosity to dissipate heat and store water and high specific heat capacity, allowing them to effectively alleviate the urban heat island effect[3,4].

Permeable pavements can be made from a variety of materials, including grass, blocks or porous materials such as porous asphalt and concrete, which are widely used due to their multifunctional nature[4]. However, the use of cement promotes environmental pollution, mainly through the emission of carbon dioxide. Furthermore, in the cement manufacturing process, limestone, shale, and clay are prepared, dried, crushed, mixed, and heated in cement kilns at temperatures of up to 1200 °C to 1450 °C to produce clinker, resulting in high energy costs as seen in the recent review by Mohamad et al.[5]. In the case of permeable concrete pavements, to obtain improved mechanical resistance, one alternative is to increase the cement content, as in the work of Ulfiana et al.[6], who required 17 to 26% cement in their permeable pavements, obtaining the best mechanical resistance values for the higher cement contents, contributing to greater pollution due to the increased cement content.

A new kind of permeable pavement that has been recently researched, as seen in the work of Castillo-Rodríguez et al.[7], is permeable ceramic pavement, which presents excellent, well-developed hydraulic and mechanical properties, such as good resistance to wear and compression, dispensing with the use of cement, which in its production also promotes environmental pollution, as seen in the recent review by Mohamad et al.[5]. However, the high price of these materials and the complexity of the production process limit their large-scale application[4].

One way to significantly reduce the cost of ceramic flooring is through the use of waste such as mineral waste that has chemical elements similar to the original raw materials of ceramic formulations, which can even improve the quality of some products, in addition to alleviating problems with environmental impact and sustainability of mineral extraction companies, which generate waste, which according to Zeng et al.[8], mineral exploration and ecological environmental protection often come into conflict in urban agglomerations, due to the enormous demand for mineral resources for economic growth versus the search for sustainability by local governments in many parts of the world.

Recent studies highlight the potential of mineral waste for the manufacture of ceramic materials used in civil construction such as Figueirêdo et al.[9] reported that waste

*e-mail: r.ramosf30@gmail.com
Associate Editor: Celso Santilli.
Editor-in-Chief: Luiz Antonio Pessan.

from the exploitation and processing of scheelite can be used in ceramic formulations for semi-porous tiles and porcelain tiles when calcined at 1200 and 1250 °C, respectively. Almeida et al.[10] produced environmentally friendly formulations based on scheelite and kaolin wastes for the manufacture of ceramics tiles and porcelain stoneware. Caetano et al.[11] studied ceramic formulations containing kaolin and granite processing wastes and porcelain polishing wastes to produce ceramic tiles and demonstrated that the products could be classified as ceramic tiles.

Based on these previous studies, this work proposes the use of kaolin processing residue, scheelite processing residue, granite processing residue and red clay to produce permeable ceramic pavements. The use of these wastes, which are abundant and geographically close in the Borborema Plateau (Paraíba, Brazil), allows for reduced transportation costs and minimizes the environmental impacts of mining.

The objective of this study is to develop and characterize porous ceramic formulations for application in sustainable permeable floors and pavements, seeking to balance high porosity (>40%), good mechanical flexural resistance (>2 MPa), and low production cost. This approach aims to contribute to efficient urban drainage and the utilization of industrial byproducts, offering a technically viable, environmentally responsible, and economically competitive alternative to conventional concrete pavements.

2. Materials and Methods

To produce ceramic materials, it is necessary to evaluate the factors that influence processing, which according to Barba et al.[12], have four main factors: mass composition; particle size distribution and shape; degree of compaction before firing, called compactness; and firing conditions.

When evaluating, according to studies, the influence of compaction pressure[13], heating speed[14] and granulometry[15] with the aim of producing high porosity, it is necessary to use low compaction pressure, granulometry with more spacing between particles and low heating speed to facilitate the formation of pores and formation of more resistant phases, maintaining porosity.

2.1. Raw materials

The raw materials used were obtained from the Borborema Province in northeastern Brazil, which mainly encompasses the states of Paraíba (PB) and Rio Grande do Norte (RN): Kaolin waste (KW) from the exploitation of Zoned Pegmatite in the Equador-RN region; Scheelite waste (SW) from the exploitation of Tactite in the Currais Novos-RN region; Granite waste (GW) from the exploitation of Zoned Pegmatite in the city of Várzea-RN; and commercial red clay (RC) from a deposit located in Santa Luzia-PB.

2.2. Characterization of raw materials

Initially, the chemical characterizations and mineral phases of the raw materials were performed using X-ray fluorescence (EDX 720 – Shimadzu) and X-ray diffraction (XRD600 – Shimadzu), using CuKα radiation (λ = 1.54 Å), operated at 40 kV and 30 mA, in the angular range of 2θ from 5 to 60° and a step size of 0.02°. The particle size distribution was carried out by laser diffraction granulometry in wet mode (1064, CILAS) for all raw materials. The residues were used without grinding to enable more economical processing routes, avoiding high costs and facilitating their commercial utilization.

2.3. Production of the samples

The raw materials were dried in an oven at 100 °C (Orion 515 model, FANEN A-H-T controller) and classified using an 80-mesh sieve (180 μm). In this way, 20% of the kaolin exhaust was used, with most of it being fine with more clay minerals. For the other residues, scheelite and granite, as well as red clay, practically 100% were used because they have a finer grain size.

The formulated compositions and their respective nomenclatures are described in Table 1 and were suggested to compare the types of flooring in proportions with the same proportion of each (33.33%) and in proportions with equal contents of each (40%) and lower clay mineral content (20%), also having a formulation with the same proportion of each residue 25% of each.

The formulations were prepared by dry mixing in a ball mil in 30 rmp (CFW 08 Weq) for 24 hours, using 0.5% oleic acid as a lubricant agent. Then, the mixtures were moistened with 10% distilled water and stored in plastic bags for 24 hours to ensure moisture homogenization.

The specimens were shaped using a uniaxial pressing machine (Ribeiro 15 ton) at 20 MPa in a rectangular mold of 60 × 20 mm. For the analysis of the flow test, specimens with dimensions of 120 × 60 mm were produced. After pressing, they were dried at room temperature for 24 hours, followed by drying in an oven at 100 °C for 24 hours. Subsequently, all specimens were sintered in a controlled furnace (FLYEVER FE 500 RP) at 1050 °C, 1100 °C, and 1150 °C, with a heating rate of 5 °C/min and a dwell time of 60 minutes.

As stated in the work of Segadães[16], the influence of the oxides present in the residues changes the phases formed in the three-phase phase diagrams such as the silica-alumina-calcium oxide diagram, silica-alumina-iron oxide, tending to form phases of resistance at lower temperatures than if there were no such oxides, such as the formation of anorthite and mullite.

These temperatures in the present study were chosen based on this analysis of the phase diagrams, on tests in formulations at 1000 °C that did not obtain adequate burning and based on the literature in which more satisfactory values were obtained, mainly for strength and porosity above 1000 °C up to 1150 °C for kaolin and granite residues Caetano et al.[11] and with scheelite residues Almeida et al.[10] and Figueirêdo et al.[9].

Table 1. Formulated compositions and nomenclatures for the samples produced.

Formulations (wt. %)	Raw materials			
	KW	SW	GW	A
K1	33	0	33	33
K2	40	0	40	20
S1	0	33	33	33
S2	0	40	40	20
A	25	25	25	25

It should be noted that no tests or care with heavy metals were necessary, since these residues do not contain them, and tungsten was not detected in the scheelite residue (CaWO4) in X-ray diffraction. Thermal analyses were also not necessary, since these residues are known in the literature, as seen in the work of Fernandes et al.[17]. And in addition, thermal analyses usually go up to 1000 °C, with formulations being prepared above 1050 °C.

2.4. Characterization of samples after sintering

The sintered samples were characterized by X-ray diffraction (Shimadzu, XRD-6000, CuKα radiation) for the identification of crystalline phases and by scanning electron microscopy (SEM, TESCAN) for microstructural analysis. The linear shrinkage (LS) was determined by measuring the length variation on sample before and after sintering. Physical properties such as water absorption (WA), apparent density (AD), and apparent porosity (AP) were measured based on the Archimedes principle, using distilled water as the immersion medium. The loss on ignition (LOI) was determined to evaluate the elimination of volatile materials and the thermal stability of the formulations. The three-point flexural strength (FS) was determined using a universal testing machine (Shimadzu, Autograph AGX-50 KN) with a 5 kN load cell, a support span of 40 mm, and a loading speed of 0.5 mm/min.

The flow tests were conducted using a homemade system depicted in Figure 1. The container was filled with a 5 cm high water column to calculate the permeable volume, measured in relation to time. The measurement of 5 cm (50 mm) corresponds to 50 liters per square meter, representing the water accumulation equivalent to heavy rainfall at a flow rate of 50 mm/h. The test was performed after the samples had been immersed in water for 24 hours.

For the calculation of the permeable flow, the formula of Equation 1 was used, in which J is the liquid flow; V is the permeated volume; A is the area through which the water infiltrates; and Δt is the permeation time:

$$J = \frac{V}{A\ddot{A}t} \quad (1)$$

For the thermal expansion and moisture expansion test, test specimens with dimensions of 50x10x5 mm were used. The linear expansion coefficient was determined using an RB 3000 dilatometer from RB Engenharia in the temperature range of 30 °C to 600 °C.

For the moisture expansion test, samples were reheated at 550 °C for 2 hours, then immersed in boiling water for 24 hours and reheated at a rate of 2 °C/min to 550 °C for 2 hours and cooled in a dilatometer. The difference in the hysteresis of this last heating cycle is the moisture expansion of the samples.

The wear evaluation of the tiles was performed through the Mohs hardness test, comparing with mineral standards and correlating with the results of the Calowear micro-abrasion test, following the methodology of Gonçalves et al.[18].

3. Results

Figure 2a shows the particle size distribution, and Figure 2b shows the particle size frequency distribution of the raw

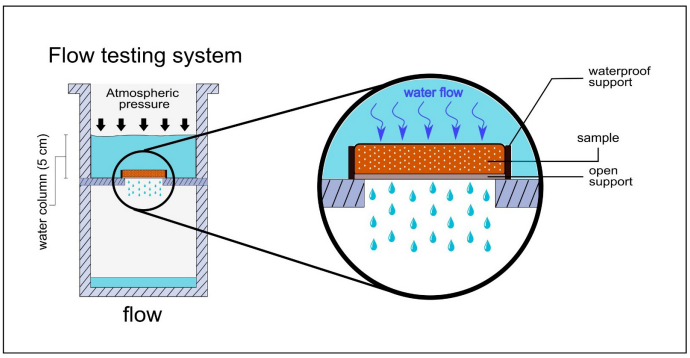

Figure 1. Diagram of the permeability test used for the two floors with the best results.

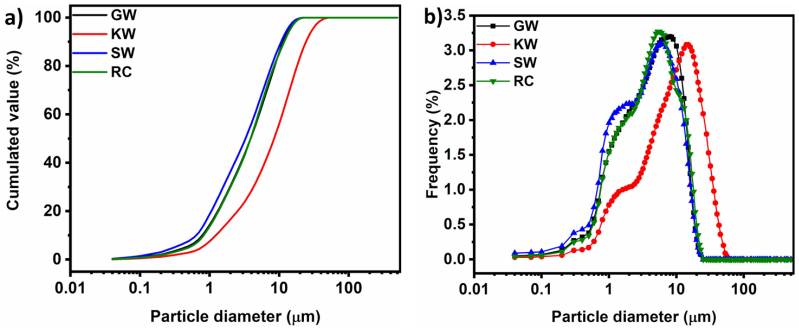

Figure 2. Particle size distribution curve from sieving (a), particle size distribution curve from laser granulometry (b), and particle size frequency distribution curve from laser granulometry (c) for raw materials used in pavement production.

materials obtained by laser particle size measurement. The red clay and the wastes presented homogeneous distribution curves (Figure 2a) and bimodal particle size distribution curves (Figure 2b). Despite the presence of fines related to kaolinite particles, KW presents larger particles than the other residues. The particle sizes ranged from approximately 1 to 24 μm for KW, with an average diameter of 10.9 μm; from 0.6 to 11 μm for SW, with an average diameter of 4.6 μm; and from 0.8 to 11 μm for GW and RC, with an average diameter of 5.1 μm.

Table 2 summarizes the granulometric distribution of the raw materials used, indicating that GW, SW, and red clay (RC) presented narrower particle size distribution than KW.

Table 3 presents the chemical compositions of the raw materials. SW is mainly composed of calcium oxide (CaO) (59.4% by weight), with other constituents such as silica (SiO2) (20.3% by weight), alumina (Al_2O_3) (7.5% by weight), iron oxide (Fe_2O_3) (6.1% by weight), magnesium oxide (MgO) (4.2% by weight), and potassium oxide (K_2O) in smaller quantities. The high CaO content is associated with the presence of calcite.

The main constituents of KW were SiO_2 (53.7% by weight) and Al_2O_3 (38.8% by weight), also containing Fe_2O_3 (1.0% by weight), K_2O (5.3% by weight), and MgO (1.1% by weight) in smaller amounts. GW consists of a high amount of SiO_2 (59.4% by weight) with other oxides in smaller amounts, such as Al_2O_3 (18.0% by weight), Fe_2O_3 (7.7% by weight), CaO (5.3% by weight), MgO (3.1% by weight), and K_2O (3.8% by weight). While RC is composed of a high amount of SiO_2 and Al_2O_3 and lower contents of Fe_2O_3 (3.2–8.4% by weight), MgO (0.6–3.1% by weight), and K_2O (0.3–4.6% by weight), which may act as fluxing oxides, in addition to CaO (2.5% by weight), due to the presence of calcium montmorillonite.

From the X-ray fluorescence results seen in Table 3 and the percentage of materials for each formulation, according to Table 1, the percentages of oxides in each formulation are calculated, as can be seen in Table 4. From these results it is possible to analyze the ceramic phase diagrams recommended by Segadães[16] for formulations with many oxides such as mineral residues, using the three-phase diagram containing silica (SiO_2), alumina (Al_2O_3) and the sum of the other fluxing oxides.

It can be seen in Table 4 that the formulations K1 and K2 are very similar in the proportions of oxides, since the kaolin residue has several components similar to the granite residue, diverging in their mineralogical phases, since the kaolin residue has levels of the clay mineral kaolinite, influencing the formation of resistance phases.

Formulations S1 and S2 have no significant divergence, mainly in the calcium oxide contents, influencing the formation of pores mainly by the decarbonation of calcite. Formulation A presents a very interesting composition of oxides, with much higher calcium oxide contents than formulations K, still having relevant contents of alumina and silica, tending to form mullite, which is a very resistant and refractory ceramic phase, normally formed from 1200 °C, being the only aluminosilicate phase possible to form under normal pressure conditions[19].

Figure 3 presents the XRD patterns of the raw materials. In the granite waste, graph crystallographic phases corresponding to orthoclase (JCPDS 00-019-0931), quartz (JCPDS 00-046-1045), and muscovite (JCPDS 00-002-0044) were found, which are the main minerals in the mineral, as observed by Hudson-Edwards[20]. Furthermore, the presence of the hornblende phase (JCPDS 00-021-0149) is also observed as the main accessory mineral.

Table 2. Particle diameters of raw materials used for pavement production.

Raw materials	D_{10}	D_{50}	D_{90}	D_m
KW	1.2	8.4	24.4	10.9
SW	0.6	3.3	10.7	4.6
GW	0.8	3.9	11.3	5.1
RC	0.8	3.9	11.8	5.1

Table 3. Chemical composition (% by mass) of raw materials used for pavement preparation.

Raw materials	SiO_2	Al_2O_3	Fe_2O_3	CaO	MgO	K_2O	Others
KW	53.7	38.8	1.0	0.0	1.1	5.3	0.1
SW	20.3	7.5	6.1	59.4	4.2	1.2	1.3
GW	59.4	18.0	7.7	5.3	3.1	3.8	2.7
RC	53.0	26.5	8.4	2.5	3.1	4.6	1.9

Table 4. Chemical composition (% by mass) of pavements formulations.

	SiO_2	Al_2O_3	Fe_2O_3	CaO	MgO	K_2O	Outros
K1	55.36	27.76	5.70	2.60	2.43	4.57	1.57
K2	55.84	28.02	5.16	2.62	2.30	4.56	1.50
S1	44.23	17.33	7.40	22.40	3.47	3.20	2.70
S2	42.48	15.50	7.20	26.38	3.54	2.92	2.86
T	46.60	22.70	5.80	16.80	2.88	3.73	2.05

Meanwhile, the scheelite waste demonstrated the predominant presence of calcite (JCPDS 01-085-1108) as the main crystallographic phase. In addition to quartz (JCPDS 00-046-1045), muscovite (JCPDS 00-002-0044), and, in smaller quantities, dolomite (JCPDS 00-036-0426) and amphibole (JCPDS 01-073-1135). This composition reflects the effectiveness of the dense beneficiation process of skarns (the ore source of scheelite) used in the region, concentrating the scheelite (denser), while the lower-density minerals, such as calcite and dolomite, the main constituents of this type of rock, are discarded in the tailings[21].

The kaolin waste, on the other hand, is predominantly composed of kaolinite (JCPS 00-001-0527), microcline (00-019-0926), quartz (JCPDS 00-046-1045), and muscovite (JCPDS 00-002-0044). The high presence of kaolinite in the waste is associated with the beneficiation systems used in the Borborema Pegmatitic Province, which have low effectiveness in concentrating this mineral[22].

In the red clay, kaolinite (JCPS 00-001-0527), illite (JCPDS 00-002-0050), and quartz (JCPDS 00-046-1045) phases, as well as feldspars like microcline (00-019-0926), were observed. Crystalline phases similar to those found by Hoppe et al.[23].

Figure 4 presents the X-ray diffractograms of the fired samples with higher waste contents (K2 and S2) and with 25% of each material (A), sintered at 1050 °C, 1100 °C, and 1150 °C. For the formulation containing KW (sample K2), the increase in temperature promotes the decrease of peaks related to potassium feldspar (JCPDS 01-084-0710) and anorthite (JCPDS 00-010-0360) and the emergence of incipient peaks of the mullite phase. This fact is observed in the ternary phase diagrams, such as SiO_2-Al_2O_3-Fe_2O_3, with the only aluminosilicate phase possible to form under normal pressure conditions[24].

Similar results were found in studies with kaolin, scheelite, and granite residues[11] and with the increase in temperature to 1150 °C was observed a reduction in the intensity of the peaks of the feldspar phases (potassium and anorthite) and an increase in amorphous fractions, indicating a decrease in the crystallinity of the sample, mainly due to the vitrification associated with the feldspathic phases[25].

For the formulation containing SW (sample S2), in addition to characteristic peaks of anorthite (JCPDS 01-071-0748), muscovite (JCPDS 00-002-0044), and quartz (JCPDS 00-046-1045), the high content of CaO, along with MgO, FeO, and SiO_2, favored the formation of the diopside phase (JCPDS 01-089-0837), as shown in Figure 5. As the temperature increases, the peaks corresponding to muscovite and anorthite diminish, while those associated with diopside intensify, suggesting the consumption of the original phases and the progressive crystallization of CaO-MgO-SiO_2-based phases[26]. At 1100 °C, peaks near the anorthite region become more prominent at 1150 °C, indicating the crystallization of the mullite phase (JCPDS 00-015-0776).

In the case of formulation A, the presence of anorthite (JCPDS 01-071-0748), quartz (JCPDS 00-046-1045), potassium feldspar (JCPDS 01-084-0710), and diopside (JCPDS 01-089-0837) was identified (Figure 6). These phases exhibited behavior similar to that observed in formulation S2. However, when comparing the intensities of the diopside

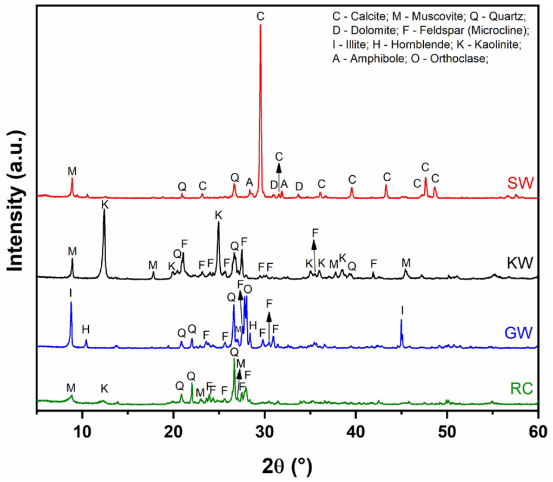

Figure 3. XRDs of residues and red clay.

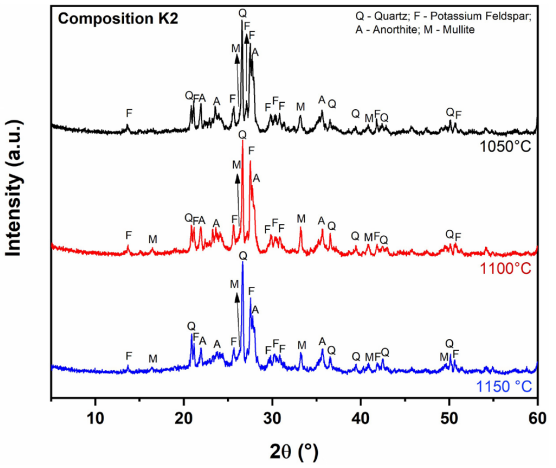

Figure 4. Diffractograms of composition K2 at different temperatures (1050 °C, 1100 °C and 1150 °C).

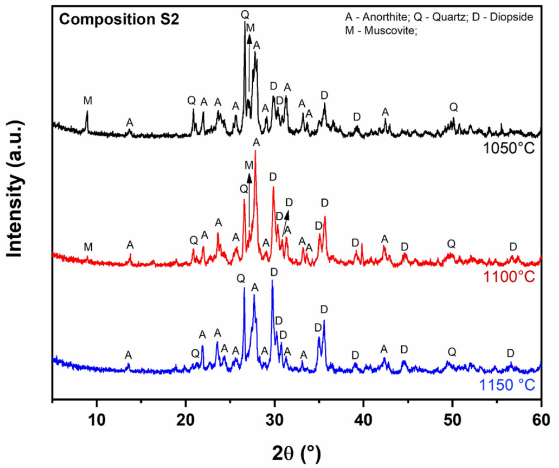

Figure 5. Diffractograms of composition S2 at different temperatures (1050 °C, 1100 °C and 1150 °C).

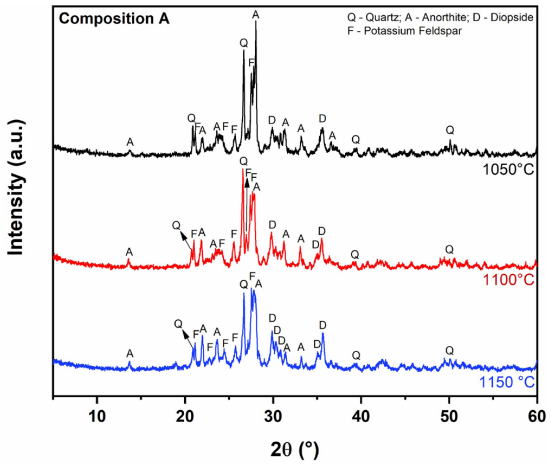

Figure 6. Diffractograms of composition A at different temperatures (1050 °C, 1100 °C and 1150 °C).

peaks in formulations S2 and A at 1150 °C, a lower intensity was noted in formulation A, which may be attributed to the presence of potassium feldspar delaying the formation of diopside. Nevertheless, in both formulations, the availability of CaO and MgO in a SiO_2-rich matrix clearly promotes the formation of the diopside phase at this temperature.

Figure 7 shows SEM images of representative unfractured surfaces of the K2 (a,b), S2 (c,d), and A (e,f) compositions after sintering at 1150 °C. It is noted that formulations S2 and A present a greater quantity of pores than formulation. This mainly occurs due to the decarbonation of calcite and the densification of the samples is not sufficient to close these pores, maintaining a certain quantity.

Structures compatible with anorthite[27] and prismatic structures, similar to mullite, as indicated in previous studies[9] can also be observed. Additionally, denser regions, associated with the vitreous phase, can be seen, as observed in the works of Teixeira et al.[28,29]. In all formulations, a

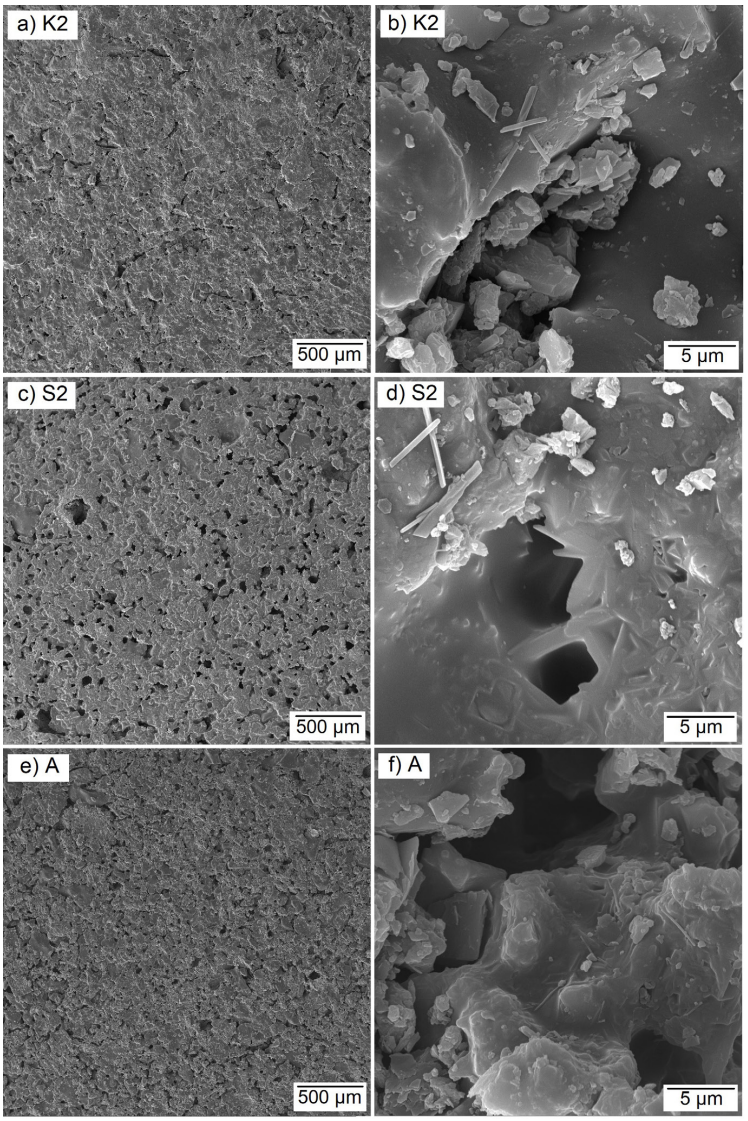

Figure 7. SEM images of the surface of samples K2 (a,b), S2 (c,d) and A (e,f) sintered at 1150 °C.

homogeneous surface is noted, with deep pores evenly distributed, which may facilitate liquid permeability.

Figures 8a-c shows results for linear shrinkage, loss on ignition, and apparent density of the samples studied. The samples containing SW (S1 and S2) show greater expansions at lower temperatures, which can be explained by the thermal decomposition of calcite and dolomite. This process causes volumetric expansion and consequent dimensional variation in the specimens, mainly due to the elimination of gases (especially CO_2), a phenomenon also observed in studies on ceramics containing carbonates[29]

A considerable increase in linear shrinkage in samples with higher sintering temperatures (1150 °C) is observed mainly in formulations with KW (K1 and K2). This is related to the formation of high-temperature crystalline phases such as mullite, anorthite as evidenced in the XRD diffractograms (Figures 4, 5 and 6).

The apparent density and loss of ignition of the samples tends to increase with temperature, which can be explained by the elimination of pores and the structural rearrangement of the ceramic matrix with new phases formation. However, formulations with SW (S1 and S2) exhibited a relatively constant apparent density, as there is a balance between volumetric expansion and mass reduction verified in the loss on ignition.

Apparent porosity (AP), water absorption (WA), and flexural strength (FS) are presented in Figures 9a-c. The K formulation, mainly K1, obtained the highest values for AP and WA, reaching 40.97% and 20.65%, respectively at 1050 °C. This is attributed to the particle size distribution of KW, which, despite having

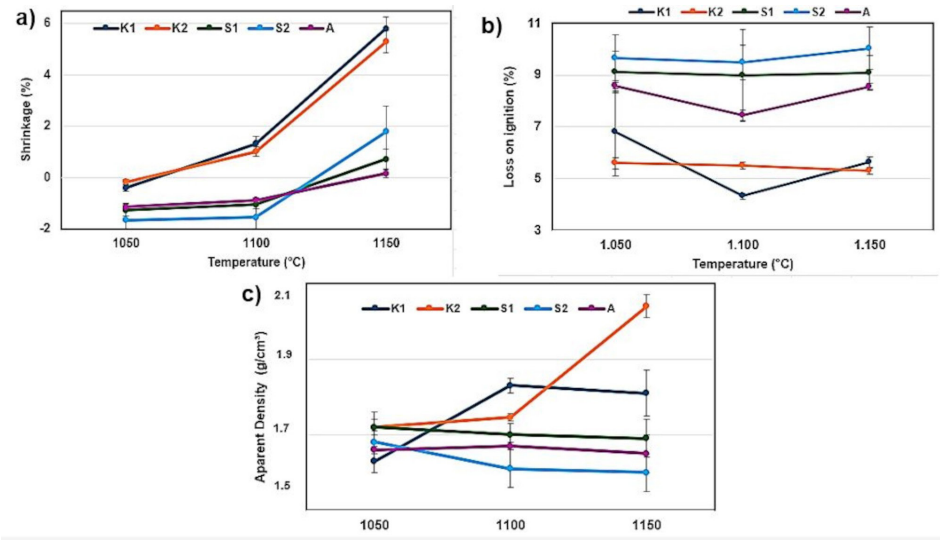

Figure 8. Results of (a) Linear contraction, (b) loss on ignition and (c) apparent density of the samples studied.

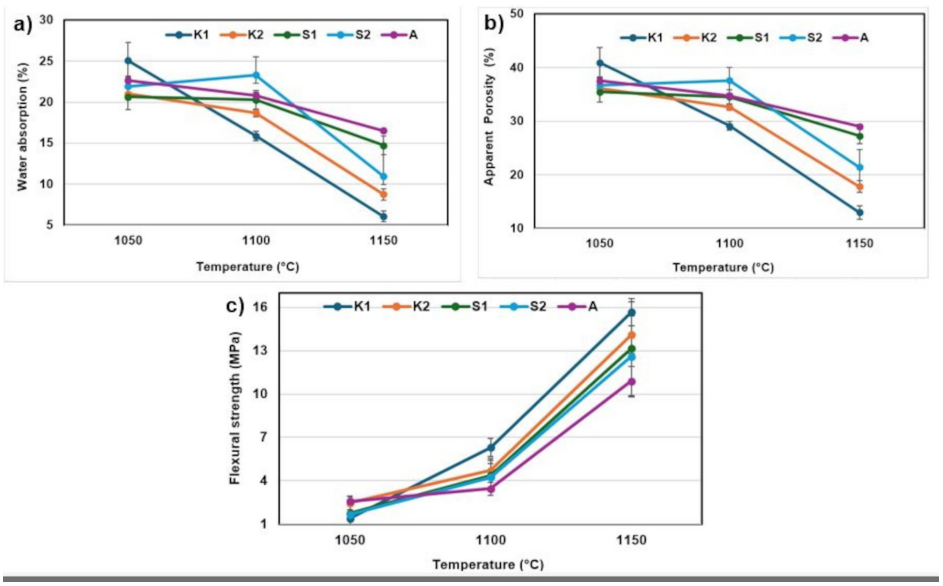

Figure 9. Results of (a) Apparent porosity, (b) water absorption and (c) flexural strength of the samples studied.

fine kaolinite particles, also has larger particles of quartz and mica. As the temperature increases, the pores close due to the formation of new phases such as vitreous phases, mainly due to the high amounts of potassium feldspar present in KW and GW, as observed in previous studies[11].

Formulations S, mainly S2, show an increase in porosity even with the increase in temperature from 1,050 °C to 1,100 °C, showing that calcite decarbonation continues even with the increase in the formation of resistance phases, as evidenced in the XRDs. With the increase in temperature to 1,150 °C, the formation of resistance phases acts more actively, promoting pore closure, but still maintaining porosity, as seen in the SEM of Figure 7c.

The formulation A presents an interesting combination of the porogenic agents of the scheelite residue and the characteristics of the kaolin residue, with no major changes occurring in its porosity even at 1.150 °C, presenting the highest values, being close to 30%, , the greatest porosity at this temperature in relation to other formulations, mainly due to having a lower flux content, in this case granite residue.

The increase in temperature promotes an increase in the flexural strength as is showed in Figure 8f for all the samples. The highest values were obtained for the formulations with KW (K1 and K2), which have higher contents of alumina and silica, resulting in greater mullite formation. Samples containing SW (S1 and S2) also showed a significant increase in strength, as anorthite phases that formed also contribute to this factor[17,30].

These porous ceramic materials can be used on permeable floors or pavements. Recent studies recommend a mechanical strength of around 2 MPa for light traffic[31] based on international standards ACI Committee, 2010, and ASTM C78-09 - 2010. According to Kia et al.[32] the ACI 325 standard (1991) states that the flexural strength for pavements should reach 3.9 MPa before being opened to road traffic, consistent with the recommendation from the Virginia Department of Transportation, USA (1997), of 3.5 MPa. For this study, all samples at 1100 °C meet this criterion.

The thermal decomposition of calcite present in SW favors the formation of larger pores[33,34], which is interesting for application in porous pavements. However, it is not enough to simply determine the pore size and the morphology for adequate water drainage and to ensure the functional performance of the material, as there must be a connection between the pores[35].

Table 5 presents the values obtained for the permeable flow test, thermal expansion coefficient, moisture expansion, and abrasion coefficient for the K1 (1050 °C) and S2 (1100 °C) floors. In the permeability test, for the K1 floor, it took 2 minutes and 45 seconds for 782.80 mL of water to infiltrate, resulting in a flow rate of 4.744 mL/s. For the S2 floor, infiltration was faster, with a time of 2 minutes and 38 seconds for the entire 50 mm water column to infiltrate completely, corresponding to a volume of 844.45 mL and a flow rate of 5.34 mL/s.

According to Barbosa and Moura[36], permeability coefficients in the range of 10^{-4} to 10^{-5} m/s are classified as medium permeability and considered adequate for use in permeable floors and pavements. Moreover, studies conducted by Jabur et al.[37], using the ASTM C1701 standard to compare permeability coefficients of soils and the results of permeability tests on permeable pavements in their research, showed that materials such as crushed gravel and sand have coefficients within the recommended range (10^{-4} to 10^{-5} m/s). Therefore, the results obtained for the K1 and S2 floors confirm their feasibility for application in permeable pavements, aligning with the guidelines and standards established in the literature.

As reported by Martino and Boschi[38], the thermal expansion of polyphase materials is influenced by the microstructure (porosity, microcracks, anisotropy), as well as by the present phases. The porous phase affects the thermal expansion of ceramic bodies in materials with coarse granulometry, high porosity (>30%), and characteristics of anisotropic expansion. This dependence of thermal expansion on porosity and granulometry justifies the low thermal expansion coefficients observed in the floors up to 100 °C, with values of 27.7 x 10^{-7} $°C^{-1}$ for K1 and 43 x 10^{-7} $°C^{-1}$ for S2. The lower thermal expansion coefficient of the K1 floor can be attributed to its microstructural phases and total porosity

The thermal expansion coefficients of floors from ambient to 500 °C are within the range of values observed for silicon-based porcelains (40 – 70 × 10^{-7} $°C^{-1}$) and ceramics containing mullite (50 – 70 × 10^{-7} $°C^{-1}$)[39]. These results indicate that the K1 and S2 floors exhibit thermal behavior compatible with reference ceramic materials, demonstrating potential for applications requiring resistance to moderate thermal variations.

The obtained values for ME are also consistent with other ceramic formulations, as observed by de Menezes et al.[40] who determined moisture expansion values of up to 0.095% in one of their samples. However, the higher value obtained in this work was lower than 0.06%, a value considered limiting for the application of floor tiles[40].

Regarding wear resistance, according to Gonçalves et al.[18] the wear coefficient can be equivalent to the Mohs hardness standards of ceramic materials. By substituting the wear value of the standard mineral Kc into the wear coefficient equation, the equivalent coefficient Ke is obtained. In the case of the K1 formulation, with a hardness of 4.5, it is observed in literature[18] a value of lnKc of -23 for SiC. By substituting into the formula for the wear coefficient of standard minerals in the silicon carbide test the Ke value of 4.7 m^2/N is obtained.

Table 5. Technological tests for samples of floor K1 and S2.

Pavements	Permeable flow (m/s)	Thermal expansion coefficient ($°C^{-1}$)	Moisture expansion (%)	Wear coefficient Ke. (m^2/N).
K1 (1050°C)	6.6 x 10^{-4}	27.7 x 10^{-7*} 46 x 10^{-7**}	0.040	4.7
S2 (1100°C)	7.42x10^{-4}	43 x 10^{-7*} 69 x 10^{-7**}	0.059	6.07

Values of the coefficient of thermal expansion for *30°C – 100°C; **100°C – 550°C.

For the S2 floor, which exhibited a hardness of 6.5 Mohs, the calculated wear coefficient Ke was 6.068 m^2/N, a value consistent with those reported for similar ceramic formulations by Gonçalves et al.[18]. It is noteworthy that, despite containing high-strength and high-hardness phases, the K1 floor presented lower hardness than S2. This can be attributed to the lower sintering temperature of 1050 °C, at which fewer crystalline phases, responsible for improving the mechanical strength of ceramic bodies formed. The K1 sample, being more suitable for pedestrian traffic, displayed significantly lower wear compared to the S2 floor, which is more appropriate for light vehicular traffic due to its higher wear coefficient.

These permeable ceramic pavements have advantages even when compared to some types of pavements that do not have porosity, in which infiltration occurs through the empty spaces between the concrete blocks, as these empty spaces cause an irregularity in the floor that is felt during vehicle driving[4]. It is also possible to reduce the size of the pores in ceramic pavements by increasing the temperature, as verified in the work of Firmino et al.[30], making it possible to obtain pores with diameters on the order of 5μm, hindering the passage of larger impurities.

Thermal energy is the main source of energy needed to produce traditional ceramics, representing up to 97.62% of the energy needs in the ceramic industry. However, it is possible to achieve savings even in the distribution of pieces in the kilns, such as the type of stacking and firing position, potentially saving up to 30% of energy[41]. Thus, a challenge for the processing of ceramic paving is undoubtedly the firing temperature, which, with the decrease in clay minerals and feldspars, tends to need to be increased to obtain greater strength, as observed in formulation S2.

This firing temperature can be reduced by grinding the waste, tending to obtain higher strengths, even at lower temperatures, since the surface area between the particles is greater; however, grinding increases the cost of ceramic processing by 15 to 20%[42]. To obtain satisfactory ceramic products, temperatures above the metakaolin formation stage are necessary above 900 °C[43], resulting in more resistant crystalline phases, as well as greater densification through particle sintering. Therefore, the need for a small increase in temperature (from 1050 °C to 1100 °C) to achieve higher resistance values may be insignificant in relation to grinding costs[7].

4. Conclusions

The results obtained in this study demonstrate that the developed ceramic formulations have great potential for application in permeable floors, meeting the mechanical resistance and porosity requirements necessary for this functionality. Thermal and microstructural characterization showed that porosity and granulometry directly influence the thermal expansion and moisture expansion of the floors. The wear assessment indicated that the formulations have durability compatible with commercial ceramic floors. Formulations containing kaolin waste, especially K1, achieved high porosity (40.97%) and bending strength of 2.45 MPa at 1050 °C, making them suitable for applications where efficient drainage is a priority and mechanical stresses are low. As for the formulations containing sheelite waste, the S2 formulation, sintered at 1100 °C, stood out with a bending strength of 4 MPa and porosity close to 40%, demonstrating a better balance between strength and permeability, making it suitable for light traffic applications.

Thus, this work provides a scientific contribution to studies of permeable ceramic floors, showing that the use of various parameters to increase porosity and facilitate chemical reactions improved the results, offering a low-cost permeable floor with performance comparable to commercial concrete floors.

5. Acknowledgments

The authors would like to thank the National Council for Scientific and Technological Development – CNPq, for the financial support granted to the research projects (nº 407848/2022-3 and 309771/2021-8), the Financing Agency for Studies and Projects – FINEP (project no. 01.22.0251.00), and the Paraíba State Research Support Foundation – FAPESQ (Announcement 06/2021, project no. 3064/202). They would also like to thank the companies that provided the waste used in this study, as well as the Federal University of Campina Grande – UFCG, for the institutional support and financial support.

6. References

1. Woods Ballard B, Wilson S, Udale-Clarke H, Illman S, Scott T. The SUDS manual. London: CIRIA.
2. Alsubih M, Arthur S, Wright G, Allen D. Experimental study on the hydrological performance of a permeable pavement. Urban Water J. 2017;14(4):427-34. https://doi.org/10.1080/1573062X.2016.1176221.
3. Fang M, Wang X, Liu J, Xu Z, Chen Y. Design, application and performance improvement of Eco-Permeable pavement materials (Eco-PPMs): a review. Constr Build Mater. 2022;360:129558. https://doi.org/10.1016/j.conbuildmat.2022.129558.
4. Zhou J, Pang Y, Du W, Huang T, Wang H, Zhou M, et al. Review of the development and research of permeable pavements. Hydrol Processes. 2024;38(6):e15179. https://doi.org/10.1002/hyp.15179.
5. Mohamad N, Muthusamy K, Embong R, Kusbiantoro A, Hashim MH. Environmental impact of cement production and solutions: a review. Mater Today Proc. 2022;48:741-6. https://doi.org/10.1016/j.matpr.2021.02.212.
6. Ulfiana D, Suripin, Budieny H, Parmantoro P, Wibowo S. The development of a permeable pavement from concrete bricks. IOP Conf Ser Earth Environ Sci. 2021;700(1):012060. https://doi.org/10.1088/1755-1315/700/1/012060.
7. Castillo-Rodríguez JT, Andrés-Doménech I, Martín M, Escuder-Bueno I, Perales-Momparler S, Mira-Peidro J. Quantifying the impact on stormwater management of an innovative ceramic permeable pavement solution. Water Resour Manage. 2021;35(4):1251-71. https://doi.org/10.1007/s11269-021-02778-7.
8. Zeng P, Liang L, Duan Z. Ecological and environmental impacts of mineral exploitation in urban agglomerations. Ecol Indic. 2023;148:110035. https://doi.org/10.1016/j.ecolind.2023.110035.
9. Figueirêdo JMR, Costa FP, Fernandes JV, Rodrigues AM, Neves GA, Menezes RR, et al. Development of scheelite tailings-based ceramic formulations with the potential to manufacture porcelain tiles, semi-stoneware and stoneware. Materials. 2020;13(22):5122. https://doi.org/10.3390/ma13225122. PMid:33202868.
10. Almeida EP, Carreiro MEA, Rodrigues AM, Ferreira HS, Santana LNL, Menezes RR, et al. A new eco-friendly mass formulation based on industrial mining residues for the manufacture of ceramic tiles. Ceram Int. 2021;47(8):11340-8. https://doi.org/10.1016/j.ceramint.2020.12.260.
11. Caetano ALA, Marques VC, de Macedo DA, Ferreira HS, Dutra RPS, Menezes RRN. Obtenção de cerâmica de revestimento

sustentável desenvolvida com resíduos industriais. Ceram Ind. 2021;26(1):1-11. https://doi.org/10.4322/cerind.2021.004.
12. Barba A, Beltrán V, Feliu C, García J, Ginés F, Sánchez E, et al. Materias primas para la fabricación de soportes de baldosas cerámicas. Castellón: Instituto de Tecnología Cerámica; 2002.
13. Siqueira FB, do Espírito Santo LS, Holanda JNF. Influência da pressão de compactação sobre as propriedades de massa de revestimento cerâmico poroso. Acta Scint Techn. 2015;3(2):25-9. https://doi.org/10.5935/2317-8957.20150004.
14. Silva BJDA, Gonçalves WP, Cartaxo JM, Macedo RS, Menezes RR, Neves GA, et al. Influência da taxa de aquecimento e da temperatura de queima sobre as propriedades de peças produzidas com massas da cerâmica vermelha. In: 55º Congresso Brasileiro de Cerâmica; 2011; Porto de Galinhas, PE. Anais. São Paulo: Associação Brasileira Cerâmica; 2011.
15. Prado ACA, Zanardo A, Menegazzo APM, Moreno MMT. Influência da distribuição granulométrica na estabilidade dimensional de placas cerâmicas de base vermelha. Ceramica. 2008;54(332):466-71. https://doi.org/10.1590/S0366-69132008000400013.
16. Segadães AM. Use of phase diagrams to guide ceramic production from wastes. Adv Appl Ceramics. 2006;105(1):46-54. https://doi.org/10.1179/174329006X82927.
17. Fernandes JV, Guedes DG, Costa FP, Rodrigues AM, Neves GA, Menezes RR, et al. Sustainable ceramic materials manufactured from ceramic formulations containing quartzite and scheelite tailings. Sustainability. 2020;12(22):9417. https://doi.org/10.3390/su12229417.
18. Gonçalves RA, de Mello JDB, Aguiar KM, Rosa FG. Avaliação da resistência ao desgaste de pisos cerâmicos através da resistência equivalente aos padrões de dureza Mohs. Ceram Ind. 2004;9(1):16-20.
19. Gonçalves GE, Sabioni ACS, Ferraz WB, Costa GM, Brito W, Dias JA, et al. Síntese e caracterização de mulita utilizando sílica obtida da casca de arroz. REM Rev Escola Minas. 2009;62(3):367-72. https://doi.org/10.1590/S0370-44672009000300016.
20. Hudson-Edwards KA. Geochemistry and mineralogy of wastes from lithium-bearing granite-pegmatite mining: resource potential and environmental risks. Frontiers in Geochemistry. 2024;2:1378996. https://doi.org/10.3389/fgeoc.2024.1378996.
21. Baek SH, Jeon HS. Application of jig separation for pre-concentration of low-grade scheelite ore. Mater Trans. 2018;59(3):494-8. https://doi.org/10.2320/matertrans.M2017150.
22. Leite JYP, Veras MM, Santos EP, Lima RFS, Paulo JBA, Pinheiro M. Technological characterization of kaolin tailing from small-scale mining in RN and PB states – Brazil. Miner Eng. 2007;20(9):959-61. https://doi.org/10.1016/j.mineng.2007.03.006.
23. Hoppe J Fo, Pires CAO, Leite OD, Garcez MR, Medeiros MHF. Characterization of Red Ceramic Waste for Application as Mineral Addition in Portland Cement. J Mater Civ Eng. 2021;33(6):04021108. https://doi.org/10.1061/(ASCE)MT.1943-5533.0003719.
24. Gonçalves GE, Sabioni ACS, Ferraz WB, Costa GM, Brito W, Dias JA, et al. Síntese e caracterização de mulita utilizando sílica obtida da casca de arroz. REM Rev Escola Minas. 2009;62(3):367-72. https://doi.org/10.1590/S0370-44672009000300016.
25. Zanelli C, Raimondo M, Guarini G, Dondi M. The vitreous phase of porcelain stoneware: Composition, evolution during sintering and physical properties. J Non-Cryst Solids. 2011;357(16-17):3251-60. https://doi.org/10.1016/j.jnoncrysol.2011.05.020.
26. Tulyaganov DU, Dimitriadis K, Agathopoulos S, Fernandes HR. Glasses and glass-ceramics in the CaO–MgO–SiO2 system: diopside containing compositions: a brief review. J Non-Cryst Solids. 2023;612:122351. https://doi.org/10.1016/j.jnoncrysol.2023.122351.
27. Ouali A, Sahnoune F, Belhouchet H, Heraiz M. Effect of CaO addition on the sintering behaviour of anorthite formed from kaolin and CaO. Acta Phys Pol A. 2017;131(1):159-61. https://doi.org/10.12693/APhysPolA.131.159.
28. Teixeira SR, Souza AE, Carvalho CL, Reynoso VCS, Romero M, Rincón JM. Rincón JMa. Characterization of a wollastonite glass-ceramic material prepared using sugar cane bagasse ash (SCBA) as one of the raw materials. Mater Charact. 2014;98:209-14. https://doi.org/10.1016/j.matchar.2014.11.003.
29. Soares RAL, do Nascimento RM, Paskocimas CA, Castro RJS. Efeito da adição de calcita oriunda de jazida de argila em massa de cerâmica de revestimento. Ceram Ind. 2014;19(3):27-32. https://doi.org/10.4322/cerind.2014.076.
30. Firmino HCT, Gomes DS, Silva VC, Santos IMG, Lira HL, Santana LNL, et al. Sustainable ceramic membranes from clays and mining wastes by rapid sintering process. Mater Res. 2025;28:e20240499. https://doi.org/10.1590/1980-5373-mr-2024-0499.
31. Barreto Sandoval GF, Galobardes Reyes I, Schwantes-Cezario N, Campos Moura A, Martins Toralles B. Correlation between Permeability and Porosity for Pervious Concrete (PC). Dyna. 2019;86(209):151-9. https://doi.org/10.15446/dyna.v86n209.77613.
32. Kia A, Wong HS, Cheeseman CR. High-strength clogging resistant permeable pavement. Int J Pavement Eng. 2021;22(3):271-82. https://doi.org/10.1080/10298436.2019.1600693.
33. Martínez-Martínez S, Pérez-Villarejo L, Garzón E, Sánchez-Soto PJ. Influence of firing temperature on the ceramic properties of illite-chlorite-calcitic clays. Ceram Int. 2023;49(14):24541-57. https://doi.org/10.1016/j.ceramint.2022.11.077.
34. Jiang F, Zhang L, Jiang Z, Li C, Cang D, Liu X, et al. Diatomite-based porous ceramics with high apparent porosity: pore structure modification using calcium carbonate. Ceram Int. 2019;45(5):6085-92. https://doi.org/10.1016/j.ceramint.2018.12.082.
35. Marchioni M, Becciu G. Permeable pavement used on sustainable drainage systems (SUDs): a synthetic review of recent literature. WIT Trans Built Environ. 2014;139:183-94. https://doi.org/10.2495/UW140161.
36. Barbosa RS, Moura PM. Análise da permeabilidade de pavimento intertravado vazado. In: X Encontro Nacional de Águas Urbanas; 2014; São Paulo, SP. Anais. Porto Alegre: ABRHidro; 2014.
37. Jabur AS, Dornelles F, Silveira ALLD, Goldenfum JA, Okawa CMP, Gasparini RR. Determinação da capacidade de infiltração de pavimentos permeáveis. RBRH. 2015;20(4):937-45. https://doi.org/10.21168/rbrh.v20n4.p937-945.
38. Marino LFB, Boschi AO. A expansão térmica de materiais cerâmicos. Parte I: introdução, aplicações e composição da massa. Ceram Ind. 1998;3(1-2):17-21.
39. Marino LFB, Boschi AO. A expansão térmica de materiais cerâmicos. Parte II: efeito das condições de fabricação. Ceram Ind. 1998;3(3):23-33.
40. Menezes RR, Segadães AM, Ferreira HS, Ferreira HC. Análise da expansão por umidade e absorção de água de pisos cerâmicos comerciais em relação à composição química e à quantidade estimada de fase vítrea. Ceramica. 2003;49(310):72-81. https://doi.org/10.1590/S0366-69132003000200003.
41. Vidak Vasić M. Techno-economic analysis in the service of traditional ceramic industry. The first review. Structural Integrity and Life. 2024;24(2):199-205. https://doi.org/10.69644/ivk-2024-02-0199.
42. Izak P, Delihowski J, Mastalska-Popławska J, Stempkowska A. Utilisation of mining waste for production of ceramic tiles. Appl Sci. 2025;15(7):3957. https://doi.org/10.3390/app15073957.
43. Jabr A, Škapin S, Tominc S, Daneu N, König J, Ducman V, et al. Enhancing densification of metakaolin-based geopolymers via the cold sintering process. Open Ceramics. 2025;24:100863. https://doi.org/10.1016/j.oceram.2025.100863.

Data Availability

The full dataset supporting the findings of this study is available upon request to the corresponding author: Ricardo Ramos Filho: r.ramosf30@gmail.com.